Decoding of 23 Unique Magnetic Nanobarcodes

Mohammad Reza Zamani Kouhpanji[®] 1,2, Joseph Um[®] 1, and Bethanie Stadler[®] 1

¹Department of Electrical and Computer Engineering, University of Minnesota, Minneapolis, MN 55455 USA

²Department of Biomedical Engineering, University of Minnesota, Minneapolis, MN 55455 USA

The unmet demand for data privacy and brand protection in anti-counterfeiting has urged heavyweight industries to develop new nanomaterials for barcoding. Here, we tailor the remanence spectra of magnetic nanowires (MNWs) to make 23 new unique magnetic nanobarcodes signatures. Using arrays of 30 and 100 nm diameter MNWs, composed of FeCo, Ni, or Co, we establish design rules for generating diverse codes followed by the description of a simple decoding algorithm. When used together, remanence spectra and our decoding algorithm enabled unambiguous identification of 14 of 15 combinations of two nanobarcodes. When three nanobarcodes were present at the readout simultaneously, our algorithm was able to successfully identify 9 of 20 combinations. Our approach opens a promising path toward expandable encoding and reliable decoding of MNWs.

Index Terms-Magnetic nanowires (MNWs), nanobarcoding, reliable decoding, remanence spectra.

I. INTRODUCTION

LONGATED magnetic nanoparticles, called magnetic nanowires (MNWs), have aroused much attention in diverse fields because of their outperformance functionalities in biomedical and technological applications, particularly, in biolabeling and nanobarcoding applications [1]–[4]. The three essential merits of nanobarcodes are 1) expandable encoding, 2) secure sensing, and 3) reliable decoding. The elongated morphology of MNWs grants them directional-dependent magnetic properties, also known as magnetic anisotropy. Magnetic anisotropy is a measure of how hard or easy the magnetization can be switched by applying an external field, called coercivity (H_c). As a result, the H_c became the central focus in many studies as an encoding parameter to encode MNWs suitable for biolabeling and nanobarcodes [5]–[9].

The easiest way to tune H_c in MNWs is to vary the diameter and composition [10], [11]. H_c can also be tuned by modulating the MNWs diameter (i.e., multi-diameter MNWs) [12], [13] and/or modulating the MNWs composition (i.e., multi-segmented MNWs) [14], [15]. Numerous MNW barcodes can be generated by combining the aforementioned approaches. However, the main bottleneck for implementing the MNWs in nanobarcoding applications is the lack of reliable decoding of H_c values as the identification signature, especially when there are more than one barcode at the readout [6], [16], [17]. The reason is that techniques for measuring H_c , such as hysteresis loop measurements, only provide a single value for H_c which is not sufficient for decoding [6], [18]. What is worse, the measured H_c values can be significantly different from the real values due to the interaction fields (H_u) among the MNWs. Methods such as first-order reversal curves (FORC) have been proposed to measure the H_c and H_u distributions as decoding signatures [19]. However, the FORC

Manuscript received March 1, 2021; revised June 20, 2021; accepted July 7, 2021. Date of publication July 9, 2021; date of current version January 20, 2022. Corresponding author: B. Stadler (e-mail: stadler@umn.edu).

Color versions of one or more figures in this article are available at https://doi.org/10.1109/TMAG.2021.3096169.

Digital Object Identifier 10.1109/TMAG.2021.3096169

method is significantly slower than other methods [20], which makes it impractical for decoding compared with other types of nanobarcode methods, such as traditional radio frequency identification (RFID) tags [21].

To bring MNW barcodes closer to practical applications, we recently proposed to utilize irreversible switching fields at zero applied field, which is also called remanence magnetization, as the encoding signature [16], [17], [22], [23]. Three merits make remanence spectrum particularly useful for nanobarcoding. First, since remanence spectra are measured at zero field after applying a predefined field, background noise is minimized. That is because the other materials, such as food products, are paramagnetic and diamagnetic which do not produce any magnetic signal at zero field. Second, remanence spectra can be measured significantly faster than FORC because remanence methods require significantly fewer data points. Considering the required data points, a remanence spectrum can be measured at the same time as a hysteresis loop, but it provides substantially more information. Third, the remanence spectra are a function of both H_c and H_u distributions, which enable not only an expansion of the number of codes, but also make the decoding of unknown remanence spectra plausible.

II. EXPERIMENTAL APPROACH

Several types of MNWs were electrodeposited into polycarbonate membranes using a three-electrode electrodeposition setup, and the details can be found in our previous works [4], [10]. The polycarbonate membranes were used in this study because polycarbonate is a biocompatible polymer that is used daily, including cellphone and tablet covers, personal wallets, and eyeglasses [24]. Fig. 1(a) shows the procedure for electrodepositing MNWs inside the polycarbonate membranes. For the sake of simplicity, we engineered the remanence spectra of MNWs using the coercivity (H_c), which was tuned by the MNWs diameter (30 and 100 nm) and composition (Ni, Co, and Fe65Co35). The composition determines the crystal anisotropy and saturation magnetization, the ratio of which contributes to H_c engineering. Note that these MNWs had large aspect ratios, that is, length (=2 μ m)

0018-9464 © 2021 IEEE. Personal use is permitted, but republication/redistribution requires IEEE permission. See https://www.ieee.org/publications/rights/index.html for more information.

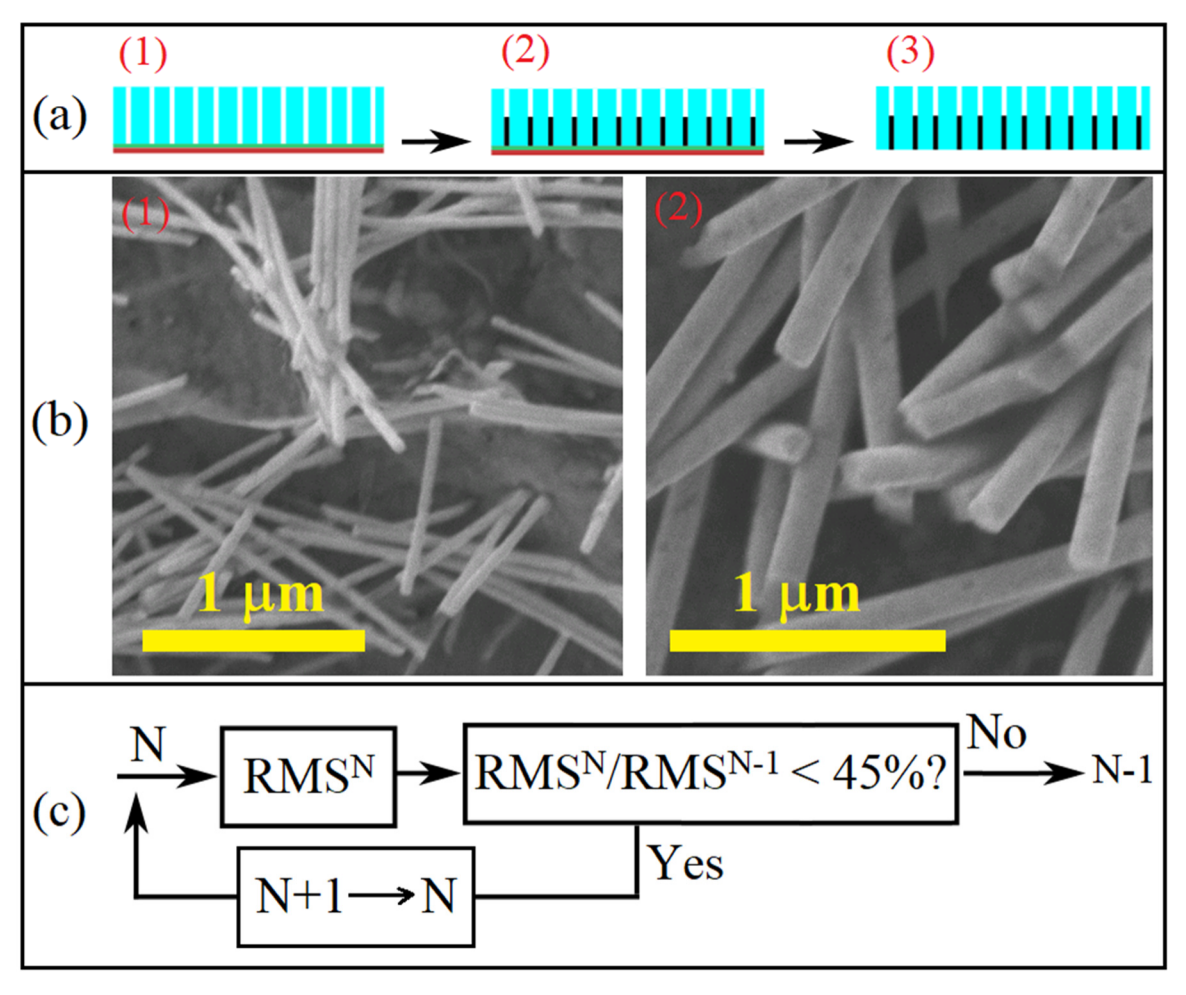


Fig. 1. (a) MNWs fabrication process: (1) evaporating back-contacts onto one side of the template, (2) electrodepositing MNWs, and (3) removing the back-contacts. (b) SEM images of MNWs, (1) 30 nm MNWs and (2) 100 nm MNWs. (c) Schematic of the decoding algorithm.

to diameter ratios; thus, the shape anisotropy contribution on H_c was the same for all cases [see Fig. 1(b)]. We chose diameters of 30 nm for large H_c and 100 nm for small H_c . It is well known that H_c of MNWs decreases as the diameter increases [25].

The remanence spectra were measured using the standard protocol of the backward remanence magnetization (BRM) method explained in [22]. The only difference between the BRM and other remanence measurements, such as isothermal and dc demagnetization methods, is that the BRM method saturates the MNWs at each step before applying and removing a field (H). This strictly controls the MNWs switching which results in a more reproducible readout that is suitable for reliable decoding. To decode an unknown remanence spectrum, it is necessary to determine the number and types of nanobarcodes in the readout. To do so, we propose an automated algorithm that uses the variation of the root-mean-square (rms) error as an indicator for decoding [26], [27]. Theoretically, any remanence spectra can be written as a summation of the integral of N Gaussian functions, defined as follows:

$$F(H) = \frac{1}{\sqrt{2\pi}} \sum_{i=1}^{N} \frac{M_{\text{sr}}^{i}}{\sigma^{i}} \int \exp\left[-\frac{1}{2} \left(\frac{\log(H) - \log(H_{\text{in}}^{i})}{\sigma}\right)^{2}\right] d\log(H)$$

where $M_{\rm sr}$, σ , and $H_{\rm in}$ are the saturation remanence, dispersion parameter, and inflection point, respectively.

The first step to decode a readout remanence spectrum is to determine whether it is composed of one nanobarcodes or several nanobarcodes—simply, what is N? Needless to say, as N increases, the rms error decreases because the fit quality improves. However, the rms error becomes constant when the readout remanence spectrum is overfitted, and the rms error will not be significantly reduced. Considering this fact, we first assume that there is only one nanobarcode (N = 1) at the readout, and the measured remanence spectrum is fit to (1) to find the parameters $(M_{\rm sr}, \sigma, \text{ and } H_{\rm in})$ by optimizing RMS1, where superscript 1 indicates N = 1. Next, N is increased to 2 and the new optimum rms error, RMS2, is calculated. Then, RMS2 is compared with RMS1 to determine how much the rms error decreased by increasing N from 1 to 2. If the reduction meets the cutoff, which was found to be 55% for our MNWs sets, then there are at least two nanobarcodes at the readout $(N \ge 2)$. Then, it is necessary to increase N to 3 and repeat the same procedure to determine whether or not there are more nanobarcodes present. However, if the reduction in RMS2 compared with RMS1 was not sufficient, the decoding process can be terminated because it would appear that only one nanobarcode was present at readout (N = 1). Note that this procedure is scalable so that it can be used to decode

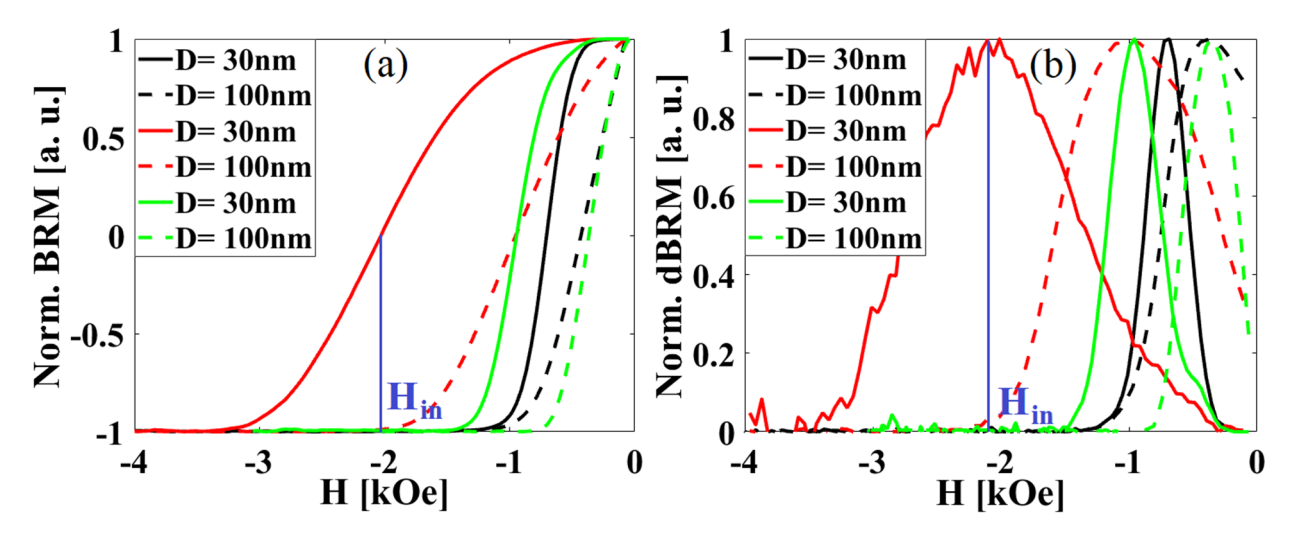


Fig. 2. (a) BRM spectra for all 6 MNW arrays. (b) Derivative of the remanence spectra with respect to the applied field (dBRM). In both subfigures, the red curves are for the Co MNWs, the green curves are for the Ni MNWs, and the black curves are for the FeCo MNWs.

TABLE I Inflection Field (H_{in}) , Coercivity (H_c) , and Saturation Remanence (M_{sr}) of the MNWs in This Study

	Ni		Со		Fe ₆₅ Co ₃₅	
	D= 30nm	D= 100nm	D= 30nm	D= 100nm	D= 30nm	D= 100nm
H _{in} [kOe]	0.931	0.345	2.019	0.889	0.696	0.366
H _c [kOe]	0.930	0.344	2.019	0.878	0.685	0.370
M _{sr} [memu]	1.34	4.497	2.382	11.86	1.273	10.05

any unknown remanence spectra composed of multiple nanobarcodes with remanence spectra. In Section III, results and discussion, we discuss this procedure to decode unknown remanence spectra composed of two and three nanobarcodes, and we provide insights on how to engineer more codes.

III. RESULTS AND DISCUSSION

Fig. 2(a) and (b) shows the normalized remanence spectra and their derivatives with respect to a predefined field (H), abbreviated as BRM and dBRM, respectively, because they were measured using the backward remanence method. We utilized the dBRM distribution because it is a good fit to a Gaussian curve, the derivative of (1). The peak of dBRM determines the inflection field (H_{in}) of the BRM. The BRM spectrum of each nanobarcode has at least one distinct feature, either its dispersion parameter (σ) or $H_{\rm in}$. We skipped the discussion of σ because we previously showed that it is not as effective as $H_{\rm in}$ for reliable decoding [17], [28]. For small interaction fields (H_u) , the absolute value of the difference between H_{in} and MNWs coercivity (H_c) is equal to H_u . For our nanobarcodes, since the average interwire distance is large (\sim 600 nm), H_u among the MNWs is negligible which results $H_{\rm in}$ to be similar to H_c .

The H_{in} values are given in Table I, where it can be seen that H_{in} decreases as the diameter of the MNWs inside

the nanobarcode increases as mentioned above. Furthermore, since Co has a larger crystal anisotropy compared with both Ni and FeCo, its H_{in} values are larger for all diameters. It is also well known that H_c of MNWs is a function of the crystal anisotropy to saturation magnetization ratio. As a result, even though Ni has a quite similar crystal anisotropy as FeCo, the 30 nm Ni has a larger H_{in} compared with the 30 nm Fe65Co35 due to its smaller saturation magnetization (485 versus 1880 emu/cc). Note that the situation is different for 100 nm MNWs because, in addition to the crystal anisotropy to saturation magnetization ratio, the exchange coefficient also impacts Hin because larger MNWs are not single domain [11], [25]. Generally speaking, MNWs with larger crystal anisotropy are magnetically more stable that means their magnetization direction does not change after applying and removing a field (H) along their easy axis. Simply, they have a higher saturation remanence $(M_{\rm sr})$, given in Table I, where Co nanobarcodes have higher $M_{\rm sr}$ owing to their larger crystal anisotropy. In summary, to expand the encoding capability of MNWs using their remanence spectra, it is essential to tailor their H_{in} , which is a strong function of the MNWs composition (crystal anisotropy and saturation magnetization and diameter). Note, here the MNWs had a uniform cylindrical geometry with a large aspect ratio (length to diameter ratio) leading to the same shape anisotropy. Interestingly, shape anisotropy has been adjusted by modulating the

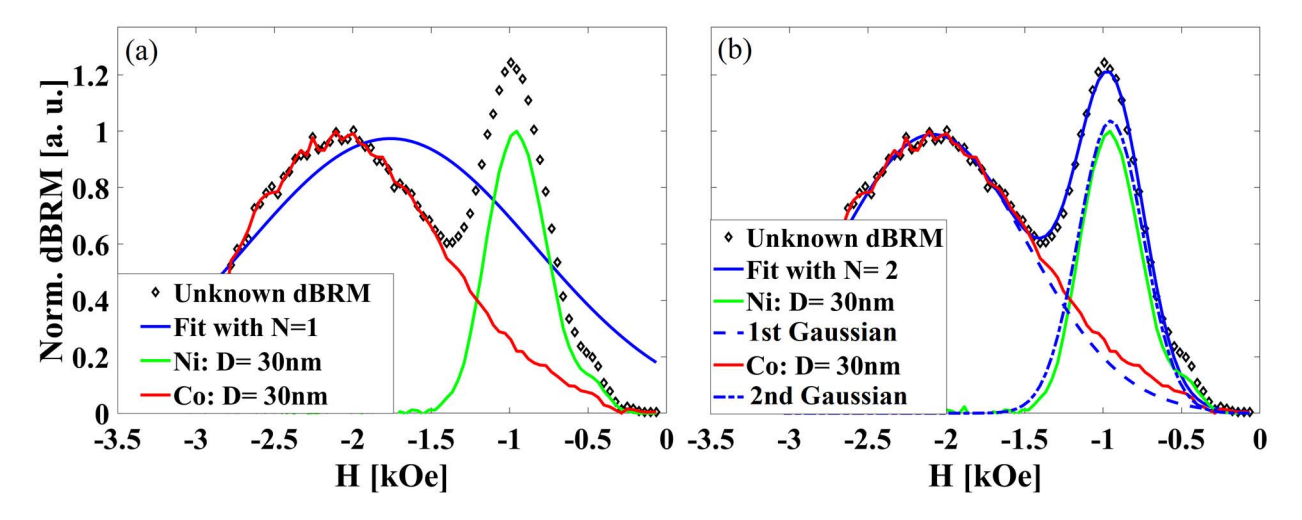


Fig. 3. Example of decoding an unknown remanence spectrum (here its derivative, dBRM, is shown) which is being decoded using our algorithm, (a) is for N = 1 in (1) and (b) is for N = 2 in (1). As can be seen, N = 1 leads to underfit (large rms) and N = 2 fits the data very well, where further increasing N causes overfit.

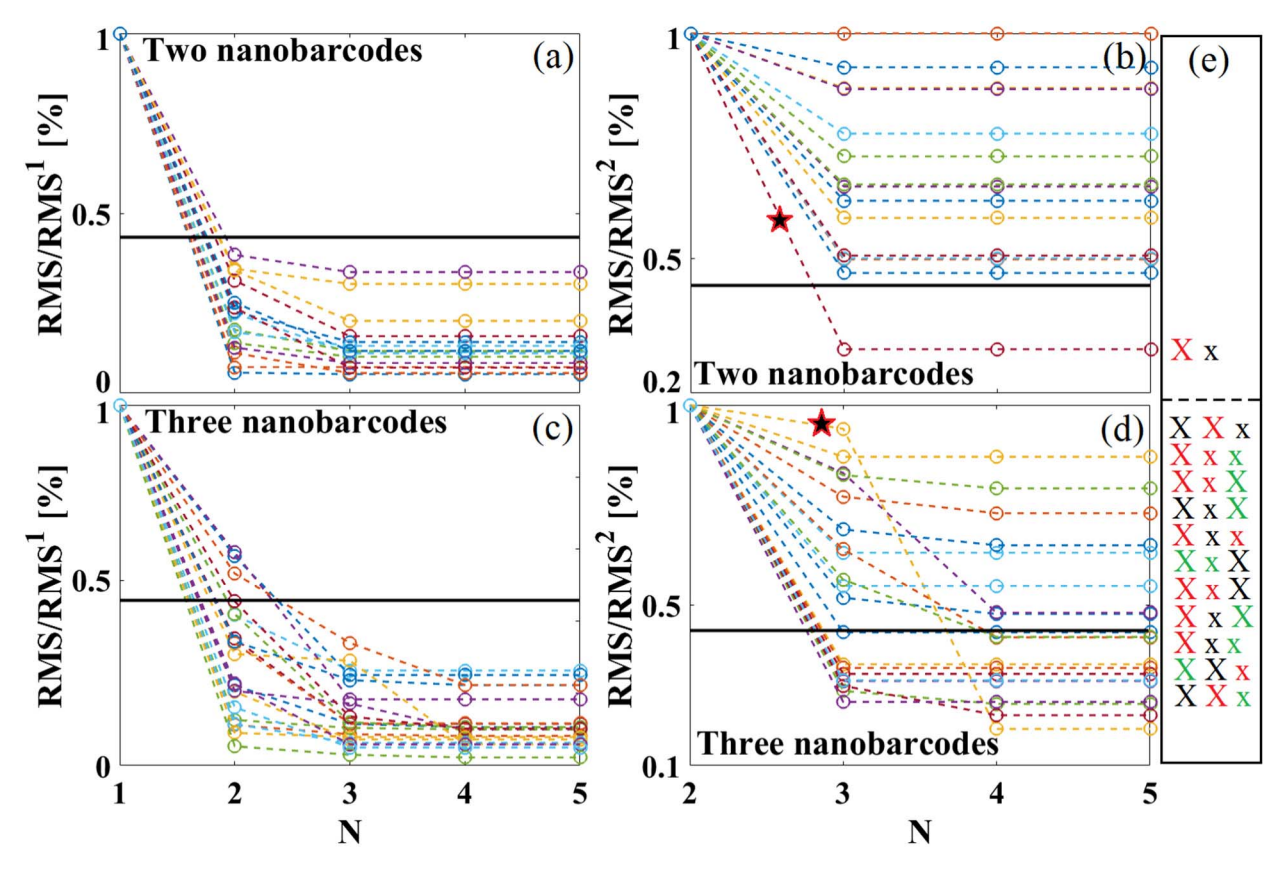


Fig. 4. Convergence curves of the decoding algorithm for (a) and (b) unknown remanence spectra composed of two nanobarcodes and (c) and (d) unknown remanence spectra of three nanobarcodes. The cutoff for the rms error is 45%, shown by solid black lines, and the unsuccessful decodings are listed (Ni = green, Co = red, FeCo = black, capital X = 100 nm diameter, small x = 30 nm diameter) at box (e). In both subfigures, the stared curves indicate an example of the failed decoding.

composition during electrodeposition [29], [30] and this could be used with our design rules for expanding MNW encoding capabilities.

As mentioned earlier, being able to generate numerous nanobarcodes with distinct codes is valuable only if the nanobarcodes can be reliably decoded. Therefore, after establishing the basic rules for expanding the encoding capability of MNWs using remanence spectra, it is vital to explore how reliably they can be decoded. Here, we employ our automated algorithm, which was described in Section II. For the sake of simplicity, we only focused on unknown remanence spectra, composed of two or three remanence spectra, even though this

algorithm can be easily adapted for unknown combinations with more nanobarcodes (N).

Fig. 3 shows an example of decoding of an unknown spectrum, shown by dots. Distinct codes are essential to have distinct peaks which lead to a large variation of rms for reliable decoding. For example, in Fig. 3, the decoding algorithm fits (1) to the data with N = 1 and calculates the rms. Then, it increases N to 2 and repeats the procedure to find the new rms. In this example, it can be clearly seen that the N=2 fits the data very well, while N=1 has a very poor fitting quality. The revolution of the rms values is shown and discussed in Fig. 4. As can be seen in Fig. 4, as N is increased during the decoding procedure, the rms error decreases till it becomes fairly constant, which means the readout remanence spectrum is being overfitted. Since the remanence spectrum of each nanobarcode may not be a perfect Gaussian distribution, reaching an exact constant rms error is not a good criterion for determining N because it overestimates N. Therefore, it is essential to establish a cutoff to indicate the line between overfit and underfit. Here, we chose the cutoff based on the ratio of the rms at each N compared with its previous rms (N-1), also called RMSN/RMSN-1. For this set of nanobarcodes, we found that the best decoding can be achieved if the rms at each step reduces at least by 55% (i.e., RMSN/RMSN-1 < 45%). Note that this cutoff value was found by try-and-error. For example, if RMS2 (fitting for N = 2) to RMS1 (fitting for N = 1) ratio is less than 45%, then there are at least two nanobarcodes and the decoding procedure must be done for N = 3. However, if the RMS2/RMS1 is larger than 45%, then there was only one nanobarcode at the readout.

According to Fig. 4(a), the RMS2 to RMS1 ratio (RMS2/RMS1) for all cases is less than 45% (solid black line), which indicates that all unknown remanence spectra contain at least two nanobarcodes. Thus, N must be increased to 3, where the RMS3/RMS2 for all cases except one [labeled by a star in Fig. 4(b) determining the combination of Co 100 nm (X) and FeCo 30 nm (x)] is larger than 45% that means it is very unlikely that the samples measured had three nanobarcodes. Therefore, the algorithm decided that there were only two nanobarcodes present, which was correct. With this method, 14 new combinations have been engineered that can be used as nanobarcodes; a high number given there was only 15 possible combinations of two nanobarcodes using our six nanobarcodes. Performing the same procedure for decoding the unknown remanence spectra composed of three nanobarcodes, the decoding was successful for another nine combinations (out of 20 possible combinations of three nanobarcodes using our six nanobarcodes). In future works, the reliability can be improved by further tailoring the remanence spectra (e.g., by making multi-segmented MNWs) or developing more solid decoding algorithms based on artificial intelligence or machine learning approaches. Our results show that using remanence spectra (measured with BRM method) of MNWs as an encoding signature not only enables an expansion in the number of generated codes, but also provides a route toward decoding unknown nanobarcodes at the readout. This decoding is something that cannot be done using a single value, such as saturation magnetization or coercivity, as proposed by previous studies.

IV. CONCLUSION

In this study, we focused on expanding the encoding capability of MNWs for nanobarcoding applications and decoding them when there was no information about the nanobarcodes at the readout. Our findings show that tailoring remanence spectra of MNWs (measured using the BRM method) is a very promising approach to generate numerous codes and has the capability to decode them. The key to decoding is the derivative of the BRM spectra (dBRM), which provides a Gaussian distribution, similar to emission spectra of optical nanoparticles. This enables a reliable decoding scheme that cannot be done using single values, such as saturation magnetization or coercivity, as proposed previously. Furthermore, the remanence spectra peak can be readily tailored by the MNWs composition and dimensions leading to the generation of diverse codes suitable for nanobarcoding applications.

ACKNOWLEDGMENT

This work was supported in part by the National Science Foundation under Grant CMMI-1762884; in part by the National Science Foundation through the National Nano Coordinated Infrastructure Network (NNCI) under Award ECCS-1542202, conducted at the Minnesota Nano Center; in part by the National Science Foundation, Earth Sciences Division, through the Instrumentation and Facilities Program, under Grant NSF/EAR 1642268, performed at the Institute for Rock Magnetism (IRM), which is a U.S. National Multi-user Facility at the University of Minnesota; and in part by NSF through the MRSEC Program, carried out in the Characterization Facility, University of Minnesota.

REFERENCES

- [1] Y. S. Jeon *et al.*, "Metallic Fe–Au barcode nanowires as a simultaneous T cell capturing and cytokine sensing platform for immunoassay at the single-cell level," *ACS Appl. Mater. Interfaces*, vol. 11, no. 27, pp. 23901–23908, 2019.
- [2] S. J. Yoon, B. G. Kim, I. T. Jeon, J. H. Wu, and Y. K. Kim, "Compositional dependence of magnetic properties in CoFe/Au nanobarcodes," *Appl. Phys. Exp.*, vol. 5, no. 10, Sep. 2012, Art. no. 103003.
- [3] M. R. Z. Kouhpanji and B. J. H. Stadler, "A guideline for effectively synthesizing and characterizing magnetic nanoparticles for advancing nanobiotechnology: A review," *Sensors*, vol. 20, no. 9, p. 2554, Apr. 2020.
- [4] M. R. Z. Kouhpanji and B. J. H. Stadler, "Projection method as a probe for multiplexing/demultiplexing of magnetically enriched biological tissues," RSC Adv., vol. 10, no. 22, pp. 13286–13292, 2020.
- [5] J. G. Fernández, V. V. Martínez, A. Thomas, V. M. de la Prida Pidal, and K. Nielsch, "Two-step magnetization reversal FORC fingerprint of coupled bi-segmented Ni/Co magnetic nanowire arrays," *Nanomaterials*, vol. 8, no. 7, pp. 1–15, 2018.
- [6] S. Shikha, T. Salafi, J. Cheng, and Y. Zhang, "Versatile design and synthesis of nano-barcodes," *Chem. Soc. Rev.*, vol. 46, no. 22, pp. 7054–7093, 2017.
- [7] J. H. Lee et al., "Iron-gold barcode nanowires," Angew. Chem.-Int. Ed., vol. 46, no. 20, pp. 3663–3667, 2007.
- [8] J. U. Cho, J.-H. Wu, J. H. Min, J. H. Lee, H.-L. Liu, and Y. K. Kim, "Effect of field deposition and pore size on Co/Cu barcode nanowires by electrodeposition," *J. Magn. Magn. Mater.*, vol. 310, no. 2, pp. 2420–2422, Mar. 2007.
- [9] M. R. Z. Kouhpanji and B. J. H. Stadler, "Magnetic nanowires for quantitative detection of biopolymers," AIP Adv., vol. 10, no. 12, Dec. 2020, Art. no. 125231.
- [10] M. R. Z. Kouhpanji and B. J. H. Stadler, "Beyond the qualitative description of complex magnetic nanoparticle arrays using FORC measurement," *Nano Exp.*, vol. 1, no. 1, Apr. 2020, Art. no. 010017.

- [11] A. Hillion, A. Tamion, F. Tournus, C. Albin, and V. Dupuis, "From vanishing interaction to superferromagnetic dimerization: Experimental determination of interaction lengths for embedded Co clusters," *Phys. Rev. B, Condens. Matter*, vol. 95, no. 13, pp. 1–11, Apr. 2017.
- [12] G. D. Sulka, A. Brzózka, and L. Liu, "Fabrication of diameter-modulated and ultrathin porous nanowires in anodic aluminum oxide templates," *Electrochim. Acta*, vol. 56, no. 14, pp. 4972–4979, May 2011.
- [13] J. A. Fernandez-Roldan, R. Perez del Real, C. Bran, M. Vazquez, and O. Chubykalo-Fesenko, "Magnetization pinning in modulated nanowires: From topological protection to the 'corkscrew' mechanism," *Nanoscale*, vol. 10, no. 13, pp. 5923–5927, 2018.
- [14] M. S. Salem et al., "Composition and diameter modulation of magnetic nanowire arrays fabricated by a novel approach," *Nanotechnology*, vol. 29, no. 6, Feb. 2018, Art. no. 065602.
- [15] C. Bran, M. Vázquez, E. Berganza, M. Jaafar, E. Snoeck, and A. Asenjo, "Magnetic imaging of individual modulated cylindrical nanowires," in *Magnetic Nano- and Microwires*. Amsterdam, The Netherlands: Elsevier, 2020, pp. 455–489.
- [16] M. R. Z. Kouhpanji and B. J. H. Stadler, "Unlocking the decoding of unknown magnetic nanobarcode signatures," *Nanosc. Adv.*, vol. 3, no. 2, pp. 584–592, 2021.
- [17] M. R. Z. Kouhpanji and B. Stadler, "Magnetic nanowires toward authentication," *Part. Part. Syst. Characterization*, vol. 38, no. 2, Feb. 2021, Art. no. 2000227.
- [18] M. R. Z. Kouhpanji, J. Um, and B. J. H. Stadler, "Demultiplexing of magnetic nanowires with overlapping signatures for tagged biological species," ACS Appl. Nano Mater., vol. 3, no. 3, pp. 3080–3087, Mar. 2020.
- [19] M. R. Z. Kouhpanji and B. Stadler, "Exploring effects of magnetic nanowire arrangements and imperfections on first-order reversal curve diagrams," *IEEE Trans. Magn.*, early access, May 17, 2021, doi: 10.1109/TMAG.2021.3080975.
- [20] J. Gräfe, M. Schmidt, P. Audehm, G. Schütz, and E. Goering, "Application of magneto-optical Kerr effect to first-order reversal curve measurements," *Rev. Sci. Instrum.*, vol. 85, no. 2, Feb. 2014, Art. no. 023901.

- [21] J. Um et al., "Magnetic nanowire biolabels using ferromagnetic resonance identification," ACS Appl. Nano Mater., vol. 4, no. 4, pp. 3557–3564, Apr. 2021.
- [22] M. R. Z. Kouhpanji, A. Ghoreyshi, P. B. Visscher, and B. J. H. Stadler, "Facile decoding of quantitative signatures from magnetic nanowire arrays," *Sci. Rep.*, vol. 10, no. 1, Dec. 2020, Art. no. 15482.
- [23] M. R. Z. Kouhpanji, P. B. Visscher, and B. J. H. Stadler, "Fast and universal approach for quantitative measurements of bistable hysteretic systems," *J. Magn. Magn. Mater.*, vol. 537, Nov. 2021, Art. no. 168170.
- [24] A. Kausar, "A review of filled and pristine polycarbonate blends and their applications," J. Plastic Film Sheeting, vol. 34, no. 1, pp. 60–97, Jan. 2018.
- [25] A. Aharoni, "Angular dependence of nucleation by curling in a prolate spheroid," *J. Appl. Phys.*, vol. 82, no. 3, pp. 1281–1287, Aug. 1997.
- [26] D. Heslop and M. Dillon, "Unmixing magnetic remanence curves withouta prioriknowledge," *Geophys. J. Int.*, vol. 170, no. 2, pp. 556–566, Aug. 2007.
- [27] D. Heslop, M. J. Dekkers, P. P. Kruiver, and I. H. M. Van Oorschot, "Analysis of isothermal remanent magnetization acquisition curves using the expectation-maximization algorithm," *Geophys. J. Int.*, vol. 148, no. 1, pp. 58–64, Jan. 2002.
- [28] M. R. Z. Kouhpanji et al., "Selective detection of cancer cells using magnetic nanowires," ACS Appl. Mater. Interfaces, vol. 13, no. 18, pp. 21060–21066, May 2021.
- [29] M. Layegh, F. E. Ghodsi, and H. Hadipour, "Improving the electrochemical response of nanostructured MoO₃ electrodes by Co doping: Synthesis and characterization," *J. Phys. Chem. Solids*, vol. 121, pp. 375–385, Oct. 2018.
- [30] M. Layegh, F. E. Ghodsi, and H. Hadipour, "Experimental and theoretical study of Fe doping as a modifying factor in electrochemical behavior of mixed-phase molybdenum oxide thin films," *Appl. Phys. A*, *Solids Surf.*, vol. 126, no. 1, p. 14, Jan. 2020.